

Article

Monitoring Urban Dynamics in the Southeast U.S.A. Using Time-Series DMSP/OLS Nightlight Imagery

Qingting Li ¹, Linlin Lu ^{1,*}, Qihao Weng ², Yanhua Xie ² and Huadong Guo ¹

¹ Key Laboratory of Digital Earth Science, Institute of Remote Sensing and Digital Earth, Chinese Academy of Sciences, Beijing 100094, China; liqt@radi.ac.cn (Q.L.); hdguo@radi.ac.cn (H.G.)

² Center for Urban and Environmental Change, Department of Earth and Environmental Systems, Indiana State University, Terre Haute, IN 47809, USA; qweng@indstate.edu (Q.W.); yxie1@sycamores.indstate.edu (Y.X.)

* Correspondence: lull@radi.ac.cn; Tel.: +86-10-8217-8102

Academic Editors: Yuhong He, Soe Myint and Prasad S. Thenkabail

Received: 28 April 2016; Accepted: 4 July 2016; Published: 8 July 2016

Abstract: The Defense Meteorological Satellite Program (DMSP)'s Operational Line-scan System (OLS) stable nighttime light (NTL) imagery offers a good opportunity for characterizing the extent and dynamics of urban development at the global and regional scales. However, their ability to characterize intra-urban variation is limited due to saturation and blooming of the data values. In this study, we adopted the methods of Mann-Kendall and linear regression to analyze urban dynamics from time series Vegetation Adjusted NTL Urban Index (VANUI) data from 1992 to 2013 in the Southeast United States of America (U.S.A.), which is one of the fastest growing regions in the nation. The newly built urban areas were effectively detected based on the trend analysis. In addition, the VANUI-derived urban areas with an optimal threshold method were found highly consistent with the Landsat-derived National Land Cover Database. The total urbanized areas in large metropolitan areas in southeastern U.S.A. increased from 8524 km² in 1992 to 14,684 km² in 2010, accounting for 5% and 9% of the total area, respectively. The results further showed that urban expansion in the region cannot be purely explained by population growth. Our results suggested that the VANUI time series provided an effective method for characterizing the spatiotemporal dynamics of urban extent at the regional scale.

Keywords: DMSP/OLS; urban areas; vegetation adjusted nighttime light; time series; Southeast U.S.A.

1. Introduction

Human-induced urban development has profound impacts on energy, water, pollution, and capacity of ecosystems [1]. Satellite observations have been widely used for urban land use classification at different scales. In particular, remote sensing data with high revisit frequency offer a good opportunity to measure spatiotemporal characteristics of urban development.

The nighttime light (NTL) imagery derived from the Defense Meteorological Satellite Program/Operational Linescan System (DMSP/OLS) can provide spatially explicit observations of artificial lighting sources across human settlements at night [2]. Strong correlations between DMSP/OLS NTL data and key socioeconomic variables such as population density, economic activity and energy use have been reported [3–6]. The DMSP/OLS nighttime images have been proved to be a cost-effective tool for large-scale human settlement and dynamic mapping [7–17]. The thresholding method for urban mapping from NTL data has been extensively used due to its simplicity and reasonably high accuracy [8,13–15]. In order to mitigate the impact of the blooming effect of NTL data, Imhoff et al. [8] proposed imposing a detection frequency threshold to reduce less frequently

detected lighted pixels for urban mapping. However, owing to the variety of urbanization patterns, no empirical brightness threshold is widely applicable for extracting urban areas to precisely match the actual boundary of urbanized areas [9–12]. To determine the optimal thresholds, urban areas extracted from relatively higher spatial resolution (e.g., Landsat TM imagery) have been used as supplementary information [13–15]. Meanwhile, census data was also used to determine the threshold [16]. Besides, the ability of multi-temporal NTL data to measure changes of urban areas over time was confirmed at regional and global scales [17].

However, several weaknesses of DMSP/OLS NTL data, including the saturation effect in urban cores, blooming phenomenon in suburban areas, and the radiometric inconsistency of digital number (DN) values across years, have been documented [7,11,13]. The Vegetation Adjusted NTL Urban Index (VANUI), which combines NTL and Normalized Difference Vegetation Index (NDVI) data, can reduce the effect of NTL saturation and increase the variation of NTL signal within urban areas [18]. The VANUI has been shown to be highly positively correlated with urban impervious surface [18], and has been successfully used to quantify the impervious surfaces at country and regional level [19,20]. Despite these efforts, the ability of multi-temporal VANUI data for characterizing the urbanization process was not fully assessed in previous studies.

According to the U.S. Census Bureau [21], the Southeast United States of America (U.S.A.) has experienced a large rate of population increase in comparison to other regions in the last decades. Urban expansion in this region favors low-density development that requires large areas of land to support single-family housing and extensive road networks [22]. The increase of urban areas may have a significant effect on the region's landscape and ecosystems [23]. The primary objective of this study was to quantify the spatiotemporal dynamics of urban development by analyzing changes in NTL data in Southeast U.S.A. from 1992 to 2013. In this study, we first preprocessed the time series of annual DMSP-OLS NTL data and NDVI data. The annual VANUI values were then calculated. Reference samples of built-up areas were extracted from the National Land Cover Database (NLCD) products. The VANUI images were used to extract urban areas for major metropolitans in 1992, 2000, and 2010, respectively. Finally, the spatiotemporal patterns of urbanization were analyzed at the regional level and for the 15 largest metropolitan areas in southeastern U.S.A.

2. Data and Methods

2.1. Study Area

The study area included the states of Tennessee, Mississippi, Alabama, North Carolina, South Carolina, Georgia and Florida (Figure 1), which occupied the southeastern portion of the U.S.A. The study area is mild wet with an average annual temperature of 17 °C and annual precipitation greater than 1300 mm [14]. According to the latest U.S. Census, over 58 million people were living in these seven states in 2010, 40% more than that in 1990.

According to 2010 U.S. Census data, we chose the 15 largest metropolitan areas in the Southeast U.S.A. to analyze their urban area and population changes in last two decades (Table 1). The geographic locations of the metropolitan areas are shown in Figure 1.

2.2. Dataset

The major datasets used in this study included DMSP/OLS NTL, AVHRR and MODIS NDVI data, USGS impervious surface product and population statistics. The DMSP/OLS NTL data measured lights on the Earth's surface from cities and settlements with persistent lighting, and others such as gas flares, fires, and illuminated marine vessels [15]. The data at each pixel are recorded as a digital number from 0 to 63 with a 1 km spatial resolution, spanning -180° to $+180^{\circ}$ in longitude and -65° to $+75^{\circ}$ in latitude. The annual cloud free composites were built using the highest-quality data based on a number of constraints [24]. In this study, we used time series NTL data from 1992 and 2013 covering southeastern U.S.A.

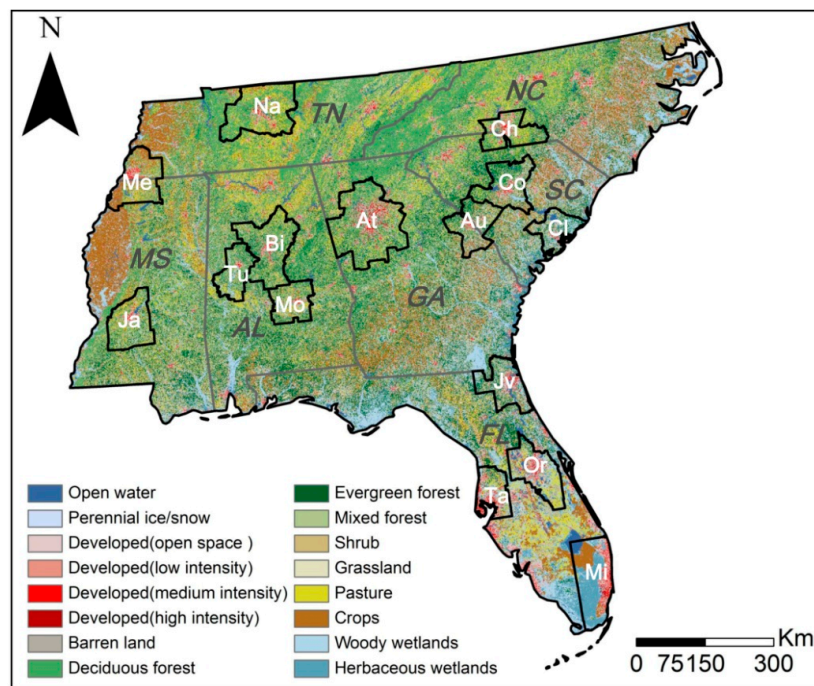


Figure 1. Land cover in the Southeast U.S.A. derived from the 2011 NLCD data set (30 m). The boundaries of the 15 largest metropolitan areas are imposed. AL = Alabama; FL = Florida; GA = Georgia; MS = Mississippi; NC = North Carolina; SC = South Carolina; TN = Tennessee.

Table 1. The 15 largest metropolitan areas in the Southeast U.S.A.

Metropolitan Area	Short Name	Area (sq km)
Atlanta-Sandy Springs-Marietta, GA	At	21,965.8
Nashville-Davidson-Murfreesboro-Franklin, TN	Na	14,925
Birmingham-Hoover, AL	Bi	13,907.6
Miami-Fort Lauderdale-Pompano Beach, FL	Mi	13,823.1
Orlando-Kissimmee-Sanford, FL	Or	10,389.6
Memphis, TN-MS-AR	Me	10,382.8
Columbia, SC	Co	9930.07
Jackson, MS	Ja	9829.24
Jacksonville, FL	Jv	8740.09
Augusta-Richmond County, GA-SC	Au	8611.35
Charlotte-Gastonia-Rock Hill, NC-SC	Ch	8150.44
Montgomery, AL	Mo	7216.77
Charleston-North Charleston-Summerville, SC	Cl	6917.13
Tuscaloosa, AL	Tu	6909.29
Tampa-St. Petersburg-Clearwater, FL	Ta	6623.5

Two NDVI data products were used in this research: MODIS 16d NDVI composite data from 2000 to 2013 and AVHRR weekly NDVI composite data from 1992 to 1999, both at 1-km spatial resolution. The MODIS NDVI data (1-km MOD13A3) were obtained from the USGS Land Processes Distributed Active Archive Center (<https://lpdaac.usgs.gov/>), and the AVHRR NDVI data were acquired from the USGS’s Earth Resources Observation and Science (EROS) Center (<https://lta.cr.usgs.gov/>). The data were radiometrically calibrated, precisely georeferenced, and corrected for atmospheric effects [25].

The National Land Cover Database is the national land cover product created by the Multi-Resolution Land Characteristics Consortium [26,27]. The NLCD 2011 Land Cover layer was used to depict background information of the Southeast U.S.A. The county level decennial census data (1990, 2000, and 2010) was also downloaded to analyze their relationship with built-up area changes.

2.3. Methodology

The proposed method for mapping the spatiotemporal patterns of urban areas included five steps (Figure 2): (1) inter-calibration of NTL and NDVI data; (2) calculation of VANUI; (3) generation of training sample; (4) extraction of built-up area for year 1992, 2000 and 2010 in metropolitan areas; and (5) the analysis of built-up area change.

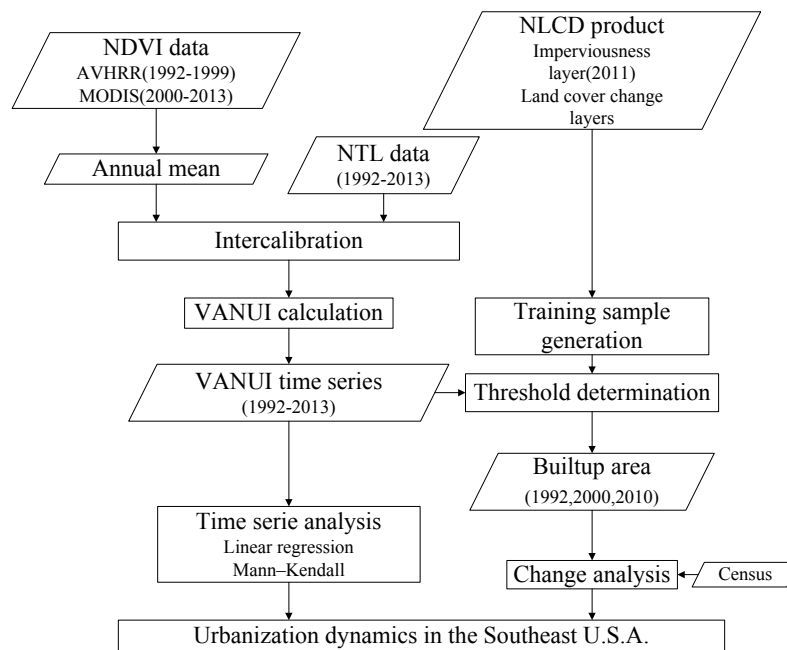


Figure 2. Procedures for mapping the spatiotemporal patterns of urbanization in the Southeast U.S.A.

2.3.1. Urban Area Extraction from NTL Data

- Data inter-calibration

In order to reduce variations and differences among sensors, an inter-calibration of NTL data was performed according to the method developed by Elvidge et al. [24]. We selected the Swain County in North Carolina as calibration area, because of its relatively stable percentage of impervious surface based on analysis of the land cover change layers. The NTL data from satellite F12 in 1999 was chosen as the reference dataset, as it had the highest cumulative DN value. A second-order regression model was developed for each satellite using Equation (1) and empirically derived coefficients by comparing the DN values from other images and reference data from satellite F12 in 1999 for Swain in North Carolina. Finally, NTL data were inter-calibrated for the period 1992–2013 using the regression model:

$$DN_{calibrated} = a \times DN^2 + b \times DN + c \quad (1)$$

where DN is the original DN value, $DN_{calibrated}$ is the intercalibrated DN value, and a , b , and c are coefficients.

The annual mean NDVI values were derived for the two NDVI products [18]. Then, all the annual mean NDVI data were projected onto an Albers Conical Equal Area projection and resampled the data to a pixel size of 1 km, based on the nearest neighbor resampling algorithm.

As a result of sensor degradation and discrepancies among different sensors, there is a lack of consistency and comparability among NDVI data in different years. The annual mean NDVI datasets were preprocessed through within- and among-sensor calibration [16]. A calibration area with high conformity to NDVI values over different years was selected and a linear regression model was used to calibrate the NDVI data from different years for the same sensor [28]. Subsequently, the inter-calibration of the NDVI data from different sensors was performed with a linear regression model [29].

- VANUI calculation

We computed VANUI in urban areas for each year from 1992 to 2013 using the following formula [18]:

$$VANUI = (1 - NDVI) \times NTL_{nor} \quad (2)$$

where NDVI is the annual mean NDVI derived from MODIS or AVHRR datasets. The NDVI values were constrained to the range of positive values between 0 and 1.0 [18]. NTL_{nor} is the normalized value of the preprocessed NTL data:

$$NTL_{nor} = \frac{NTL - NTL_{min}}{NTL_{max} - NTL_{min}}, \quad (3)$$

where NTL_{min} and NTL_{max} are the minimum and maximum values in the NTL data (0 and 63, respectively).

The VANUI values range from 0 to 1.0. Urban cores and Central Business Districts with sparse vegetation and a high lighting intensity have positive VANUI values close to 1. Peri-urban areas with lush vegetation and diffuse lighting show low VANUI values close to 0. The rationale behind using VANUI for urban area extraction is that NTL data are positively correlated with impervious surface, and vegetation abundance is inversely correlated with impervious surface [30]. Thus, the synergic use of these two types of data can improve the accuracy of estimating the spatial distribution of urban areas [31].

- Generation of training samples and the calculation of thresholds

The reference samples of built-up areas were generated using the NLCD change products. The unchanged urban pixels were extracted from the NLCD 1992–2001, 2001–2011 change products. We assumed the imperviousness of these pixels is stable during the entire study period. Their percentage impervious surface area was derived from the 2011 percentage of developed imperviousness layer. In our study, we defined built-up areas as pixels with percentage of impervious surface areas higher than 20%. The percentage of impervious surface areas of reference samples include low (20%–49%), medium (50%–79%), and high (80%–100%) (Table 2). For each metropolitan area, the threshold VANUI values to differentiate built-up areas with non built-up areas were calculated based on the training samples in the years 1992, 2000 and 2010.

- Urban area detection

With the optimal threshold value determined, the urban areas of the Southeast U.S.A. in each year were extracted from annual VANUI data in the years 1992, 2000, and 2010.

Table 2. Training samples used to determine optimized thresholds extracted from NLCD impervious surface product.

Urban Area Class	Description
Developed, Low Intensity	Areas with a mixture of constructed materials and vegetation. Impervious surfaces account for 20%–49% percent of total cover. These areas most commonly include single-family housing units.
Developed, Medium Intensity	Areas with a mixture of constructed materials and vegetation. Impervious surfaces account for 50%–79% of the total cover. These areas most commonly include single-family housing units.
Developed, High Intensity	Highly developed areas where people reside or work in high numbers. Examples include apartment complexes, row houses and commercial/industrial. Impervious surfaces account for 80%–100% of the total cover.

2.3.2. Built-Up Area Change Analysis

In this study, two methods were applied to analyze the spatial and temporal pattern of urban area change in the Southeast U.S.A. from 1992 to 2013. At the regional level, a trend analysis based on statistical methods was conducted based on VANUI time series. Specifically, a non-parametric Mann-Kendall [32] test was performed. The Mann-Kendall test has been applied to detect monotonic trends in time series for vegetation applications [33,34]. The test statistic S is computed as:

$$S = \sum_{i=1}^{n-1} \sum_{j=i+1}^n \text{sign}(y_j - y_i) \quad (4)$$

where $\text{sign}(y_j - y_i)$ is equal to +1, 0, or -1 according the positive differences, no differences and negative differences between the later-measured VANUI and all earlier-measured VANUI values. The test statistic τ can be computed as:

$$\tau = \frac{S}{n(n-1)/2} \quad (5)$$

which has a range of -1 to +1. In the two-sided Mann-Kendall test, if the null hypothesis of $\tau = 0$ is rejected, a positive value of τ indicates an increasing trend of the VAVUI in the study period. After that, the numerical trend values were retrieved to estimate trends by simple linear regression for those pixels passing the Mann-Kendall trend tests at 90% confidence level.

For metropolitan areas, the changes of urban areas were quantified based on the mapped built-up areas from VANUI data in 1992, 2000 and 2010. Their relationship with population change during the same period was analyzed based on correlation analysis.

3. Results

3.1. Regional Trend Analysis

Figure 3a shows the changing trends of pixels with significant increasing trends in the study area. Areas with significant increasing trend existed mainly in the surrounding areas of the core of metropolitan areas. As Figure 3 illustrates, the urban growth are in different spatial patterns in metropolitan areas. The newly developed built-up areas were distributed along the west northern corridors in Columbia, SC (Figure 3b). Figure 3c shows the Atlanta city was expanding in the ring form. Increasing trends were also observed for small towns scattered in this area.

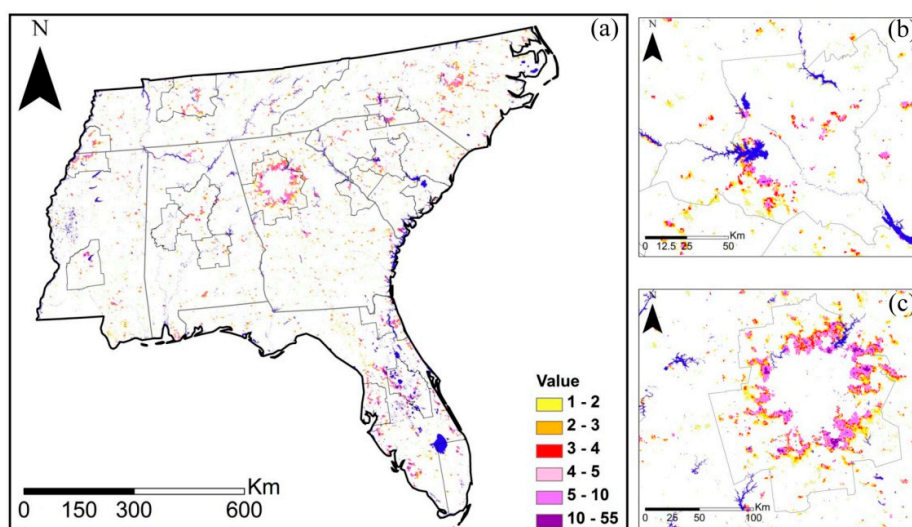


Figure 3. Changing trends (%) per year in VANUI across the Southeast U.S.A. based on the linear regression analysis, with (a) Southeast U.S.A.; (b) Columbia, SC; and (c) Atlanta, GA.

For a more comprehensive view, we chose three subsets and compared their changing trend with NLCD data (Figure 4). The changing trend of VANUI can reflect an increase of urban areas surrounding the city centers well. For small towns and villages in rural areas, the increase of low and medium density impervious surface was also revealed. However, the growth of built-up areas in central urban areas was rarely detected. For the At metro area, the changing rates of VANUI varied with regards to their distance from the urban core.

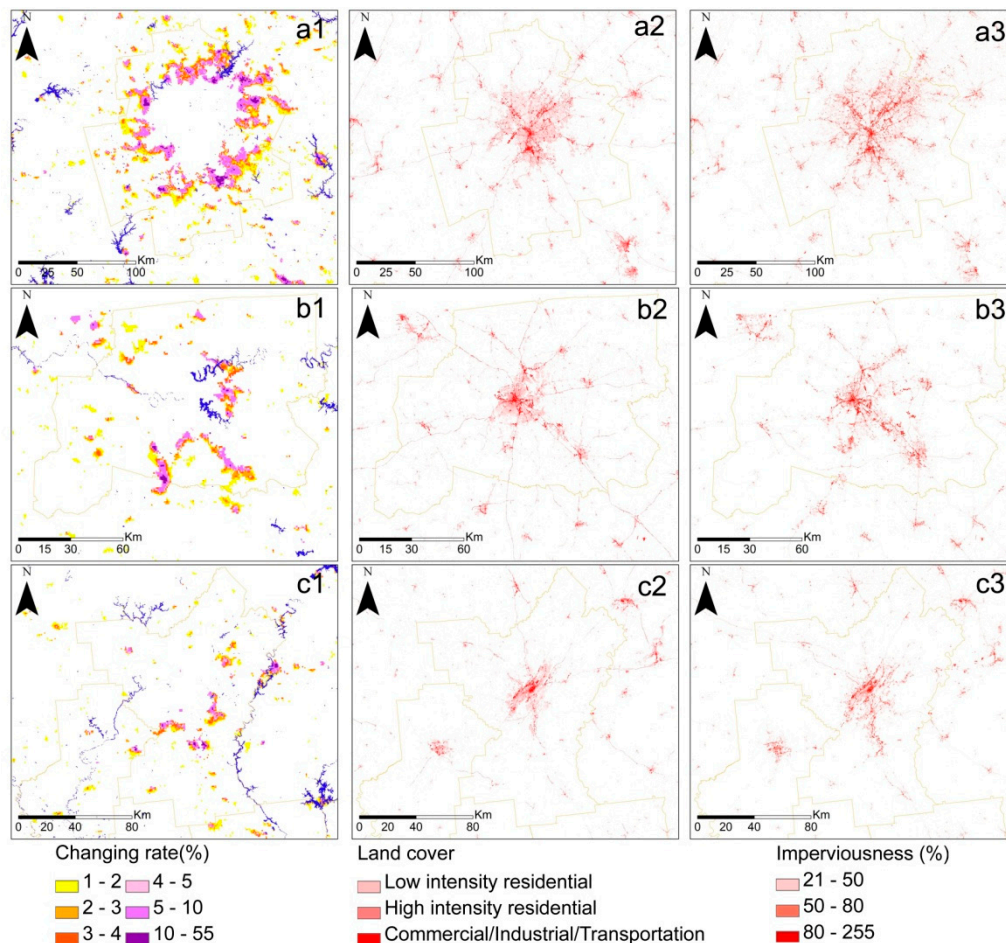


Figure 4. Comparison of VANUI changing trends with NLCD land cover products in 1992 and percentage of developed imperviousness products 2011 for three subsets. (a1–a3) Atlanta-Sandy Springs-Marietta, GA metro area; (b1–b3) Nashville-Davidson-Murfreesboro-Franklin, TN metro area; and (c1–c3) Birmingham-Hoover, AL metro area.

3.2. Built-Up Area Detection and Accuracy Assessment

We evaluated urban area detected from VANUI data with urban areas from NLCD land cover product for the Atlanta, GA metropolitan area (Figure 5). A visual comparison shows that the proposed method can map the urban extent relatively well. Due to the relatively coarse spatial resolution of NTL data, the mapped urban extent tends to be less fragmented compared to the NLCD products derived from 30 m-resolution Landsat imagery. Small size settlements in rural areas were confused with non-built-up areas due to the relatively low spatial resolution of VANUI data. The misclassification was found on boundaries of urban clusters and green space within urban clusters.

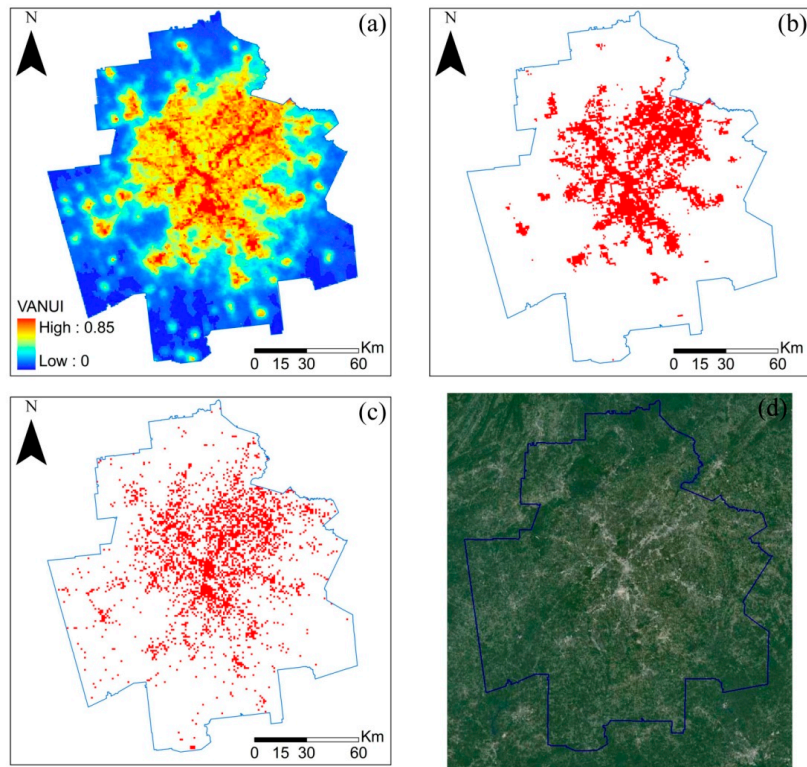


Figure 5. Urban area detection in the Atlanta metropolitan area: (a) VANUI data; (b) urban extent mapped from VANUI data; (c) urban extent from NLCD 2011 land cover product; and (d) Google Earth image.

Figure 6 shows a comparison of urban area derived from VANUI with those from the NLCD products for each metropolitan area. The NLCD products were first aggregated to 1 km resolution. The quantitative comparison indicates that our method performs well in the U.S. Southeastern region ($R^2 = 0.97$). Their difference in spatial resolution can cause their disagreement between the two datasets as observed in Figure 5. Another reason for the disagreement is their temporal discrepancy. The NLCD products are for the years 1992, 2001 and 2011, while the VANUI derived built-up areas are for the years 1992, 2000 and 2010. In order to compare urban area increase with population change, built-up areas in the same year with the decennial census data for the years 1990, 2000, and 2010 were derived.

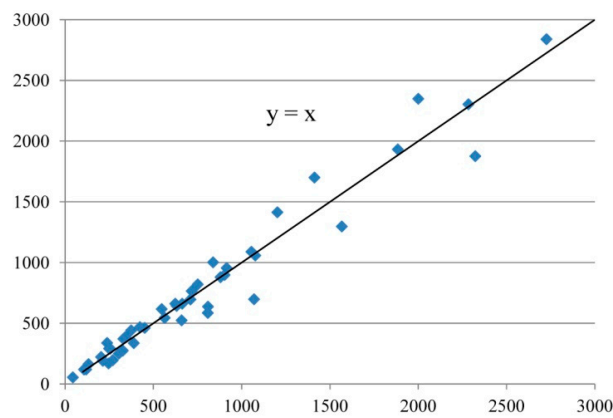


Figure 6. Comparison of urban extent (in number of 1-km resolution urban pixels) from VANUI and urban areas from USGS NLCD land cover product with linear regression in metropolitan areas in the Southeast U.S.A.

Table 3 shows the confusion matrix of VANUI-derived urban areas in 2011. The NLCD 2011 land cover product was used as ground truth data and aggregated to 1-km resolution. Pixels with percentage impervious surface areas higher than 20% were selected as built-up areas. Here, a stratified random sampling of built-up and non built-up areas was implemented. A total of 1071 sampling points consisting of 238 built-up area samples and 833 non built-up area samples were collected as validation data. The overall accuracy of 84.98% and the Kappa of 0.58 were obtained. The misclassification of built-up areas as non built-ups may be caused by the limited resolution of VANUI data in comparison to Landsat images. The non-built-up areas were mislabeled as built-up areas in urban cores due to the saturation of NTL data as the incorporation of vegetation variables cannot completely eliminate the saturation effect of NTL data in urban cores. Comparing with previous studies [15,35], the results are satisfactory at the regional level.

Table 3. Confusion matrix of built-up area extraction results from VANUI data in comparison with NLCD land cover product.

Classification	Reference Data			User's Accuracy (%)
	Built-Up	Non Built-Up	Total	
Built-up	168	91	259	64.86
Non Built-up	70	742	812	91.38
Total	238	833	1071	
Producer's Accuracy (%)	70.59	89.08		84.98

3.3. Spatiotemporal Patterns of Built-Up Area Changes in Metropolitan Areas

The changes of built-up areas were derived from VANUI data and the changes of population were generated from decennial census data (Figure 7). The total urban areas derived from the VANUI data are 8524 km² and 14,684 km² in the metropolitan areas in 1992 and 2010, respectively. The urbanized area occupies about 5% of the total area in 1992 while 9% of the total area in 2010. In 2010, the percentages of urbanized area vary from 2% in Tuscaloosa, AL metro area to 26% in Tampa-St. Petersburg-Clearwater, FL metro area. The Atlanta metropolitan area had the largest urban area in 2010, followed by Mi. The built-up area in Atlanta metro area grew at a faster rate from 1992 to 2000 than from 2000 to 2010, while the Mi metro area showed the opposite trend. Among the 15 metro areas, the Mi metro area had the largest population during the entire period. Though the Ta metro area has the smallest total area, it had the third largest built-up area and population. The Tu metro area had the smallest built-up area and population.

Built-up area differences for two periods, 1990–2000 and 2000–2010, were calculated for each metropolitan area as follows: $UB_{t1} - UB_{t2}$ ($t1:2000$ or 2010 , $t2:1990$ or 2000). Urban population (POP) differences were retrieved in the same way: $POP_{t1} - POP_{t2}$. To minimize the scale differences between the built-up area and urban population data, a data normalization scheme was applied [17,36]:

$$x_{norm} = \frac{x_i - x'}{z}, \quad (6)$$

where x_i is the built-up area or population increase of the i th metropolitan area, x' as the mean built-up area or population increase and z as the standard deviation. The normalized differences of population and urban area for metropolitan areas for two periods, 1990–2000 and 2000–2010, were plotted in Figure 8. The normalized changes of urban areas were found to be positively correlated with normalized changes in population. When At and Mi metropolitan areas were excluded, the R^2 value increased to 0.5888 (Figure 8b).

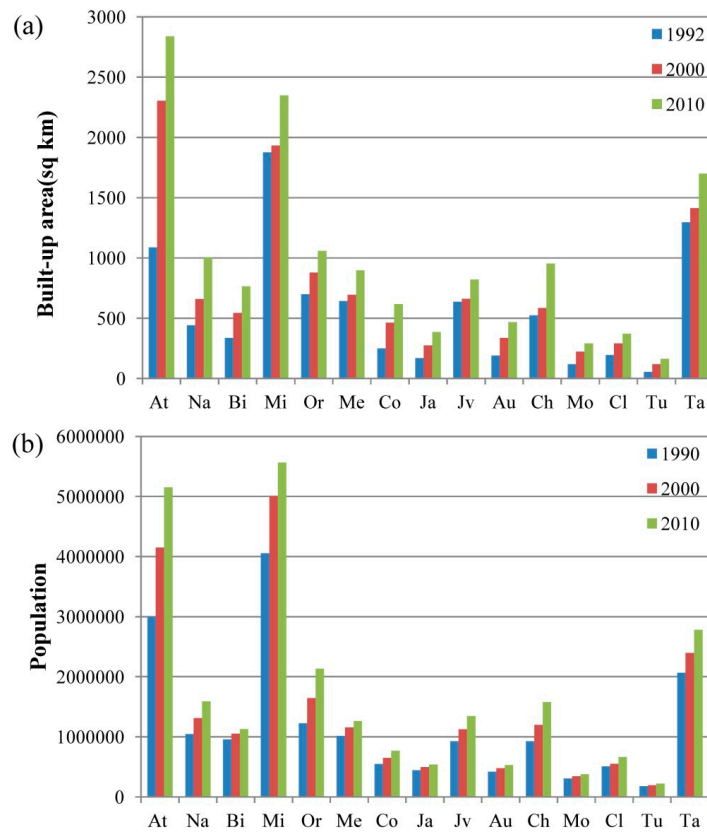


Figure 7. Changes of (a) built-up areas derived from VANUI data from 1992 to 2010 and (b) population from 1990 to 2010 in 15 metropolitan areas the Southeast U.S.A. Note: At = Atlanta-Sandy Springs-Marietta, GA metro area, Na = Nashville-Davidson-Murfreesboro-Franklin, TN metro area, Bi = Birmingham-Hoover metro area, AL, Mi = Miami-Fort Lauderdale-Pompano Beach, FL metro area, Or = Orlando-Kissimmee-Sanford, FL metro area, Me = Memphis, TN-MS-AR metro area, Co = Columbia, SC metro area, Ja = Jackson, MS metro area, Jv = Jacksonville, FL metro area, Au = Augusta-Richmond County, GA-SC metro area, Ch = Charlotte-Gastonia-Rock Hill, NC-SC metro area, Mo = Montgomery, AL metro area, Cl = Charleston-North Charleston-Summerville, SC metro area, Tu = Tuscaloosa, AL metro area, Ta = Tampa-St. Petersburg-Clearwater, FL metro area.

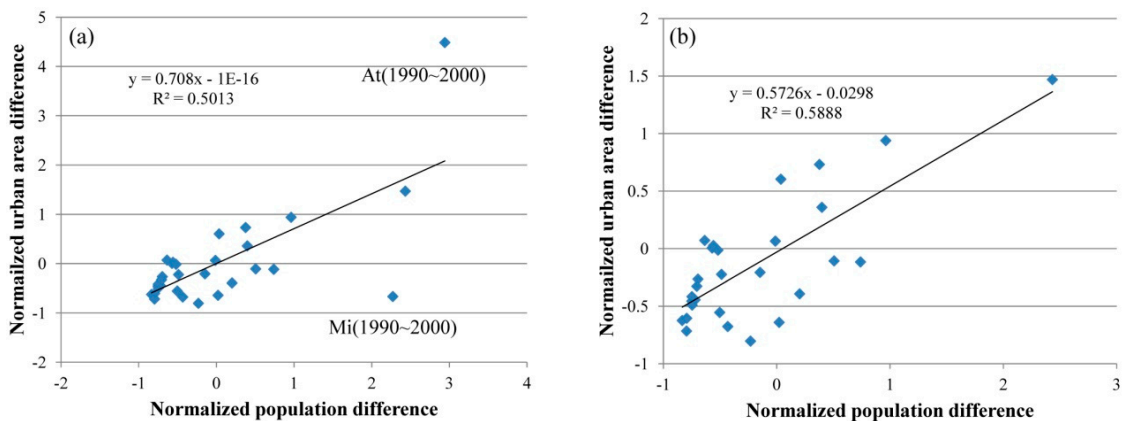


Figure 8. Changes of growth rate of population and urban areas in 15 largest metropolitan areas in the Southeast U.S.A. from 1990 to 2010. (a) All metropolitan areas were analyzed; and (b) changes in At and Mi metropolitan areas for 1990–2000 period were excluded.

An analysis based on rates of change was also conducted. The growth rate of urban population was calculated as follows: $(POP_{t_1} - POP_{t_2})/POP_{t_1}$. Urban area growth rate was calculated in the same way. The growth rates of built-up area and population were derived for the metropolitan areas for two periods: 1990–2000 and 2000–2010. A linear regression model with an R^2 of 0.0155 and p value of 0.5126 (Figure 9) suggests that the growth of urban areas derived in our study cannot be well explained by population growth and their correlation is insignificant.

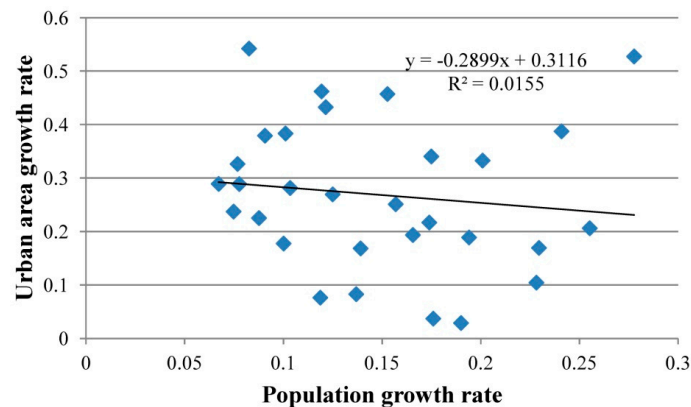


Figure 9. Normalized growth rates for urban population and nighttime lights between 1990 and 2010 for metropolitan areas in the Southeast U.S.A.

4. Discussion

This study provided an experiment for the characterization of spatiotemporal pattern of urbanization with time series DMSP/OLS NTL data. Although previous studies have showed the capacity of VANUI data to reduce the NTL saturation effect in urban cores and over-glowing effect in suburban regions [16] and to quantify regional spatiotemporal pattern of impervious surface, the studies in the application of VANUI for urbanization dynamic analysis are scarce [18].

Two methods were adopted to analyze urbanization patterns with VANUI time series, including trend analysis and thresholding method. With trend analysis, the spatial pattern of urban expansion revealed by VANUI time series matched well with the multi-temporal USGS impervious layers derived from Landsat data. Major discrepancies existed in urban center areas. According to Zhang et al. [18], the VANUI did not increase inter-urban variability of NTL values for areas with a primarily impervious surface. The uncorrected saturation of NTL in these areas may hinder the detection of urban patterns from VANUI time series. Comparing the changing rates around urban cores, the suburban regions exhibited higher changing rates than areas far from urban cores. This indicates that the areas along the urban-rural gradient had faster developing rates than rural areas.

Compared with urban areas from NLCD products, the optimal thresholds derived from the training samples for each metropolitan area can map urban extent accurately. The nightlight data tended to overestimate boundaries of large cities due to the reflectance of light from surrounding non-urban land areas [13]. Thus, some omission errors existed in suburban and rural areas. The small size settlements in these areas were not identified due to the coarse spatial and radiometric resolution of DMSP/OLS sensors, as well as their dense vegetation coverage. The linear regression model shows that the normalized population difference explained more than half of the total variation in the normalized urban area difference ($R^2 = 0.5888$). The weak correlations between growth rates of urban areas and population have been observed by Zhang et al. [8] and Zhou et al. [37]. In the southeastern U.S.A., the urbanization pattern favored suburban low-density development that required large areas of land to support single-family housing and extensive road networks [38]. Besides population change, the variance of NTL data can be related to growth of economic activities and urban land use/cover change. The difference in spatial scale between the population dataset and built-up areas may also lead to their weak correlation.

Although the VANUI time-series has been successfully adopted to explore urbanization dynamics, there are some sources of uncertainty in this study. The threshold may be improved to adapt to a larger spatial scale with larger economic variability. For example, the cluster-based optimal threshold [39] and the local SVM-based region growing method [40] can be introduced to extract urban areas with higher accuracy for regions at different development levels. Another issue, which may hinder the accuracy of extraction, was the inherent limitation of spatial and radiometric resolution of DMSP/OLS nighttime images. To address these limitations, the new generation NTL data collected from Visible Infrared Imager Radiometer Suite (VIIRS) on the National Polar orbiting Operational Environmental Satellite System (NPOESS) that provide improved measurements can be incorporated [41,42]. The integration of NTL data with data with higher spatial and spectral resolution optical image can present opportunities for better characterization of urban areas [43]. Meanwhile, combining backscatter information from microwave scatterometers with NTL data can facilitate the characterization of the structural changes of global cities and metropolitan areas [44].

5. Conclusions

In this study, we presented and evaluated methods to detect the urbanization dynamics with NTL time series in the Southeastern U.S.A. The 22 year VANUI time series were generated with inter-calibrated DMSP/OLS and NDVI data. Based on the trend analysis of VANUI, newly built urban areas can be revealed effectively. Moreover, the built-up areas can be extracted with satisfactory accuracy compared with Landsat-derived NLCD data products when optimal thresholds were applied. The total urbanized areas in the 15 largest metropolitan areas in southeastern U.S.A. increased from 8524 km² in 1992 to 14,684 km² in 2010, accounting for 5% and 9% of the total area, respectively. The results provided useful information for understanding the urbanization process in southeastern U.S.A. In addition, the relationship analysis between urban area and population change indicated that urban expansion in the region was not purely driven by population growth. In order to improve urban area mapping accuracy using DMSP/OLS NTL data, future research should explore the development of new detection methods and the integration of information from remote sensing data with higher spatial and spectral resolution.

Acknowledgments: This research was supported by the National Natural Science Foundation of China under Grant No. 41471369 and the Major Project of the National Natural Science Foundation of China under Grant No. 41590853. Q.L. and L.L. appreciated the financial assistance provided by the China Scholarship Council for supporting them for an academic visiting to University of South Carolina and for Cuizhen Wang hosting their visit.

Author Contributions: L.L. and H.G. designed the experiments; Q.L. performed the experiments; Q.W. and Y.X. helped on data analysis and writing; Q.L., Y.X. and L.L. wrote the draft.

Conflicts of Interest: The authors declare no conflict of interest.

References

1. Foley, J.A.; DeFries, R.; Asner, G.P.; Barford, C.; Bonan, G.; Carpenter, S.R.; Chapin, F.S.; Coe, M.T.; Daily, G.C.; Gibbs, H.K. Global consequences of land use. *Science* **2005**, *309*, 570–574. [[CrossRef](#)] [[PubMed](#)]
2. Elvidge, C.D.; Baugh, K.E.; Dietz, J.B.; Bland, T.; Sutton, P.C.; Kroehl, H.W. Radiance calibration of DMSP-OLS low light imaging data of human settlements. *Remote Sens. Environ.* **1999**, *68*, 77–88. [[CrossRef](#)]
3. Elvidge, C.D.; Baugh, K.E.; Kihn, E.A.; Kroehl, H.W.; Davis, E.R.; Davis, C.W. Relation between satellite observed visible-near infrared emissions, population, economic activity and electric power consumption. *Int. J. Remote Sens.* **1997**, *18*, 1373–1379. [[CrossRef](#)]
4. Sutton, P.; Elvidge, C.; Obremski, T. Building and evaluating models to estimate ambient population density. *Photogramm. Eng. Remote Sens.* **2003**, *69*, 545–554. [[CrossRef](#)]
5. Doll, C.; Muller, J.; Elvidge, C. Night-time imagery as a tool for global mapping of socioeconomic parameters and greenhouse gas emissions. *Ambio* **2000**, *29*, 157–162. [[CrossRef](#)]
6. Xie, Y.; Weng, Q. World energy consumption pattern as revealed by DMSP-OLS nighttime light imagery. *GISci. Remote Sens.* **2016**, *53*, 265–282. [[CrossRef](#)]

7. Elvidge, C.D.; Baugh, K.E.; Kihn, E.A.; Kroehl, H.W.; Davis, E.R. Mapping city lights with nighttime data from the DMSP Operational Linescan System. *Photogramm. Eng. Remote Sens.* **1997**, *63*, 727–734.
8. Imhoff, M.L.; Lawrence, W.T.; Stutzer, D.C.; Elvidge, C.D. A technique for using composite DMSP-OLS “City Lights” satellite data to map urban area. *Remote Sens. Environ.* **1997**, *61*, 361–370. [[CrossRef](#)]
9. Sutton, P.; Roberts, C.; Elvidge, C.; Meij, H. A comparison of nighttime satellite imagery and population density for the continental United States. *Photogramm. Eng. Remote Sens.* **1997**, *63*, 1303–1313.
10. Sutton, P.; Roberts, D.; Elvidge, C.D.; Baugh, K. Census from heaven: An estimate of the global human population using night-time satellite imagery. *Int. J. Remote Sens.* **2001**, *22*, 3061–3076. [[CrossRef](#)]
11. Small, C.; Pozzi, F.; Elvidge, C.D. Spatial analysis of global urban extent from DMSP-OLS night lights. *Remote Sens. Environ.* **2005**, *96*, 277–291. [[CrossRef](#)]
12. Sutton, P.C.; Cova, T.J.; Elvidge, C.D. Mapping “Exurbia” in the conterminous United States using nighttime satellite imagery. *Geocarto Int.* **2006**, *21*, 39–45. [[CrossRef](#)]
13. Henderson, M.; Yeh, E.T.; Gong, P.; Elvidge, C.; Baugh, K. Validation of urban boundaries derived from global night-time satellite imagery. *Int. J. Remote Sens.* **2003**, *24*, 595–609. [[CrossRef](#)]
14. Milesi, C.; Elvidge, C.D.; Nemani, R.R.; Running, S.W. Assessing the impact of urban land development on net primary productivity in the southeastern United States. *Remote Sens. Environ.* **2003**, *86*, 401–410. [[CrossRef](#)]
15. Liu, Z.; He, C.; Zhang, Q.; Huang, Q.; Yang, Y. Extracting the dynamics of urban expansion in China using DMSP-OLS nighttime light data from 1992 to 2008. *Landsc. Urban Plan.* **2012**, *106*, 62–72. [[CrossRef](#)]
16. He, C.; Shi, P.; Li, J.; Chen, J.; Pan, Y.; Li, J.; Li, Z.; Toshiaki, I. Restoring urbanization process in China in the 1990s by using non-radiance-calibrated DMSP/OLS nighttime light imagery and statistical data. *Chin. Sci. Bull.* **2006**, *51*, 1614–1620. [[CrossRef](#)]
17. Zhang, Q.; Seto, K.C. Mapping urbanization dynamics at regional and global scales using multi-temporal DMSP/OLS nighttime light data. *Remote Sens. Environ.* **2011**, *115*, 2320–2329. [[CrossRef](#)]
18. Zhang, Q.; Schaaf, C.; Seto, K.C. The Vegetation Adjusted NTL Urban Index: A new approach to reduce saturation and increase variation in nighttime luminosity. *Remote Sens. Environ.* **2013**, *129*, 32–41. [[CrossRef](#)]
19. Ma, Q.; He, C.; Wu, J.; Liu, Z.; Zhang, Q.; Sun, Z. Quantifying spatiotemporal patterns of urban impervious surfaces in China: An improved assessment using nighttime light data. *Landsc. Urban Plan.* **2014**, *130*, 36–49. [[CrossRef](#)]
20. Shao, Z.; Liu, C. The integrated use of DMSP-OLS Nighttime Light and MODIS data for monitoring large-scale impervious surface dynamics: A case study in the Yangtze River Delta. *Remote Sens.* **2014**, *6*, 9359–9378. [[CrossRef](#)]
21. United States Census 2010. Available online: <http://www.census.gov/2010census/> (accessed on 15 March 2016).
22. Kaza, N. The changing urban landscape of the continental United States. *Landsc. Urban Plan.* **2013**, *110*, 74–86. [[CrossRef](#)]
23. Terando, A.J.; Costanza, J.; Belyea, C.; Dunn, R.R.; McKerrow, A.; Collazo, J.A. The southern megalopolis: Using the past to predict the future of urban sprawl in the Southeast U.S. *PLoS ONE* **2014**, *9*, e102261. [[CrossRef](#)] [[PubMed](#)]
24. Elvidge, C.D.; Ziskin, D.; Baugh, K.E.; Tuttle, B.T.; Ghosh, T.; Pack, D.W.; Erwin, E.H.; Zhizhin, M. A fifteen year record of global natural gas flaring derived from satellite data. *Energies* **2009**, *2*, 595–622. [[CrossRef](#)]
25. Huete, A.; Didan, K.; Miura, T.; Rodriguez, E.P.; Gao, X.; Ferreira, L.G. Overview of the radiometric and biophysical performance of the MODIS vegetation indices. *Remote Sens. Environ.* **2002**, *83*, 195–213. [[CrossRef](#)]
26. Homer, C.G.; Dewitz, J.A.; Yang, L.; Jin, S.; Danielson, P.; Xian, G.; Coulston, J.; Herold, N.D.; Wickham, J.D.; Megown, K. Completion of the 2011 National Land Cover Database for the conterminous United States—representing a decade of land cover change information. *Photogramm. Eng. Remote Sens.* **2015**, *81*, 345–354.
27. Xian, G.; Homer, C.; Dewitz, J.; Fry, J.; Hossain, N.; Wickham, J. The change of impervious surface area between 2001 and 2006 in the conterminous United States. *Photogramm. Eng. Remote Sens.* **2011**, *77*, 758–762.
28. Teillet, P.; Holben, B. Towards operational radiometric calibration of NOAA AVHRR imagery in the visible and near-infrared channels. *Can. J. Remote Sens.* **1994**, *20*, 1–10.

29. Steven, M.D.; Malthus, T.J.; Baret, F.; Xu, H.; Chopping, M.J. Intercalibration of vegetation indices from different sensor systems. *Remote Sens. Environ.* **2003**, *88*, 412–422. [[CrossRef](#)]
30. Weng, Q.; Lu, D. A sub-pixel analysis of urbanization effect on land surface temperature and its interplay with impervious surface and vegetation coverage in Indianapolis, United States. *Int. J. Appl. Earth Obs.* **2008**, *10*, 68–83. [[CrossRef](#)]
31. Lu, D.; Tian, H.; Zhou, G.; Ge, H. Regional mapping of human settlements in southeastern China with multisensor remotely sensed data. *Remote Sens. Environ.* **2008**, *112*, 3668–3679. [[CrossRef](#)]
32. Hirsch, R.M.; Slack, J.R. A nonparametric trend test for seasonal data with serial dependence. *Water Resour. Res.* **1984**, *20*, 727–732. [[CrossRef](#)]
33. De Jong, R.; de Bruin, S.; de Wit, A.; Schaepman, M.E.; Dent, D.L. Analysis of monotonic greening and browning trends from global NDVI time-series. *Remote Sens. Environ.* **2011**, *115*, 692–702. [[CrossRef](#)]
34. Fensholt, R.; Langanke, T.; Rasmussen, K.; Reenberg, A.; Prince, S.D.; Tucker, C.; Scholes, R.J.; Bao Le, Q.; Bondeau, A.; Eastman, R.; et al. Greenness in semi-arid areas across the globe 1981–2007—An Earth Observing Satellite based analysis of trends and drivers. *Remote Sens. Environ.* **2012**, *121*, 144–158.
35. Cao, X.; Chen, J.; Imura, H.; Higashi, O. A SVM-based method to extract urban areas from DMSP-OLS and SPOT VGT data. *Remote Sens. Environ.* **2009**, *113*, 2205–2209. [[CrossRef](#)]
36. Pandey, B.; Joshi, P.K.; Seto, K.C. Monitoring urbanization dynamics in India using DMSP/OLS night time lights and SPOT-VGT data. *Int. J. Appl. Earth Obs. Geoinf.* **2013**, *23*, 49–61. [[CrossRef](#)]
37. Zhou, N.; Hubacek, K.; Roberts, M. Analysis of spatial patterns of urban growth across South Asia using DMSP-OLS nighttime lights data. *Appl. Geogr.* **2015**, *63*, 292–303. [[CrossRef](#)]
38. Brueckner, J.K. Urban sprawl: Diagnosis and remedies. *Int. Reg. Sci. Rev.* **2000**, *23*, 160–171. [[CrossRef](#)]
39. Zhou, Y.; Smith, S.J.; Elvidge, C.D.; Zhao, K.; Thomson, A.; Imhoff, M. A cluster-based method to map urban area from DMSP/OLS nightlights. *Remote Sens. Environ.* **2014**, *147*, 173–185. [[CrossRef](#)]
40. Xiao, P.; Wang, X.; Feng, X.; Zhang, X.; Yang, Y. Detecting China's urban expansion over the past three decades using nighttime light data. *IEEE J. Sel. Top. Appl.* **2014**, *7*, 4095–4106.
41. Elvidge, C.D.; Baugh, K.E.; Zhizhin, M.; Hsu, F.C. Why VIIRS data are superior to DMSP for mapping nighttime lights. *Proc. Asia Pac. Adv. Netw.* **2013**, *35*, 62–69. [[CrossRef](#)]
42. Coscieme, L.; Pulselli, F.M.; Bastianoni, S.; Elvidge, C.D.; Anderson, S.; Sutton, P.C. A thermodynamic geography: Night-time satellite imagery as a proxy measure of emergy. *Ambio* **2014**, *43*, 969–979. [[CrossRef](#)] [[PubMed](#)]
43. Huang, X.; Schneider, A.; Friedl, M.A. Mapping sub-pixel urban expansion in China using MODIS and DMSP/OLS nighttime lights. *Remote Sens. Environ.* **2016**, *175*, 92–108. [[CrossRef](#)]
44. Frohling, S.; Milliman, T.; Seto, K.C.; Friedl, M.A. A global fingerprint of macro-scale changes in urban structure from 1999 to 2009. *Environ. Res. Lett.* **2013**, *8*, 024004. [[CrossRef](#)]

